Molecular Vision 2025; 31:597-616 <http://www.molvis.org/molvis/v31/597>
Received 19 November 2024 | Accepted 29 December 2025 | Published 31 December 2025

Monocyte/macrophage-derived IL-15 activates STAT5 to trigger the EFNA1/NCOA2-positive feedback loop, facilitating retinal angiogenesis in high-glucose environments

Lixin Zhang,[1,2] Yan Guo[1,2]

[1]Department of Ophthalmology, The Affiliated Children's Hospital Of Xiangya School of Medicine, Central South University (Hunan Children's Hospital), Changsha, Hunan, China.; [2]Clinical Research Center for Pediatric Eye Diseases, Changsha, China.

Purpose: Diabetic retinopathy (DR) is of the most prevalent complications among diabetic patients. The potential role of interleukin 15 (IL-15) in modulating immune cell function and angiogenesis has drawn considerable attention. Nevertheless, the precise mechanism through which IL-15 operates in DR remains elusive.

Methods: The GSE185011 and GSE221521 data sets were harnessed to screen for upregulated genes in the blood and peripheral blood mononuclear cells (PBMCs) of patients with DR. The GSE236333 and GSE179568 data sets were used to identify upregulated genes in retinal tissues. In the clinical investigation, IL-15 was detected in T and B lymphocytes, as well as in monocytes/macrophages within the PBMCs of patients. Human retinal microvascular endothelial cells and human umbilical vein endothelial cells were either cocultured with the monocyte/macrophage cell line THP-1 under high-glucose (HG) conditions or treated with IL-15.

Results: Among the three cell types in PBMCs, monocytes/macrophages exhibited the most substantial upregulation of IL-15 under HG conditions. In vitro, IL-15 secreted by THP-1 cells augmented the STAT5 in human retinal microvascular endothelial cells and human umbilical vein endothelial cells, thereby enhancing their angiogenic potential. Inhibition of STAT5 expression counteracted the proangiogenic effect of IL-15 on endothelial cells and diminished the expression of epithelial cell adhesion molecule 1 (EFNA1). After the knockdown of nuclear receptor coactivator 2 (NCOA2), the binding affinity of STAT5 to the EFNA1 gene promoter was significantly attenuated, and the influence of IL-15 on EFNA1 expression and angiogenesis was markedly reduced. Intriguingly, knockdown of either EFNA1 or NCOA2 led to a concurrent decrease in the expression of both genes in endothelial cells, suggesting a positive feedback regulatory loop between them.

Conclusions: IL-15 secreted by monocytes/macrophages activates STAT5, which in turn induces a positive feedback regulation of the EFNA1/NCOA2 axis, ultimately promoting retinal angiogenesis under HG conditions.

Diabetic retinopathy (DR) is one of the common complications in patients with diabetes, primarily caused by prolonged hyperglycemia. This condition damages the retinal endothelial cells, leading to vascular dropout, retinal ischemia, and altered adhesion behavior of white blood cells [1,2]. As these changes occur, more factors related to angiogenesis and inflammation are produced, thereby promoting abnormal neovascularization and microvascular dysfunction. With the global number of patients with diabetes increasing, it is predicted that the prevalence of DR could reach as high as 15.7% in some regions by 2045 [3]. In developed countries, DR has become the leading cause of blindness in adults aged 20 to 74 years [4]. During this process, vascular endothelial growth factor (VEGF) plays a pivotal role, not only promoting neovascularization but also disrupting the blood-retinal barrier, indirectly driving the progression of DR. Currently, available treatments for advanced DR include corticosteroid therapy, VEGF inhibitors, and laser therapy, but these methods may bring side effects and cannot completely eliminate the risk of blindness [5]. Therefore, there is an urgent need to understand the pathogenesis in depth and to develop new therapeutic strategies.

Macrophages, as an important source of angiogenic factors, play a crucial role in promoting neovascularization [6,7]. The monocyte-macrophage family is diverse and can exhibit distinct molecular phenotypes and functions depending on different activation signals [8]. M1-type macrophages are known for their antimicrobial and proinflammatory characteristics and have the function of inhibiting angiogenesis. In contrast, M2-type macrophages play roles in tissue repair, chronic inflammation, tumor development, and angiogenesis. Recent studies have shown that succinate can induce macrophage polarization and the secretion of RBP4, which promotes neovascularization in the eye [9]. Cytokines released by macrophages, such as VEGF and tumor necrosis factor α (TNF-α), can stimulate the proliferation, migration,

Correspondence to: Yan Guo, Department of Ophthalmology, Hunan Children's Hospital, Changsha 410006, P.R. China; email: hnetyy1221@163.com

and angiogenesis of endothelial cells [10]. Additionally, the administration of interleukin (IL) 10 in the early stage of DR can protect against retinal outer barrier disruption and vascular leakage by regulating macrophage polarization [11]. Moreover, IL-17A can promote the secretion of angiogenesis-related molecules, such as VEGF and IL-6, by macrophages, thus accelerating corneal neovascularization [12]. Macrophages enhance the expression and secretion of angiogenic mediators by activating the Janus kinase (JAK2)/STAT5 and PI3K/Akt signaling pathways, thereby promoting endothelial cell migration and capillary morphogenesis, as well as inducing angiogenesis in vivo [13]. Given the significant regulatory role of macrophages in inflammation and angiogenesis, their application in ophthalmic research is increasingly recognized.

IL-15, as an inflammatory cytokine, can induce the differentiation of M1-type macrophages and plays a role in various inflammatory diseases, such as rheumatoid arthritis, psoriasis, and autoimmune diabetes [14]. IL-15 has multiple functions, including the activation of myeloid and lymphoid cells and enhancement of the innate immune response against pathogens [15]. It is primarily produced by activated macrophages, dendritic cells, and stromal cells in the bone marrow, thymus, and intestinal epithelium. The unique biosynthetic pathway of IL-15 includes its binding to IL-15Rα, followed by the transpresentation of this complex to cells expressing the IL-15Rβγ receptor [16]. When microbes activate macrophages, they rapidly produce single factors, including IL-12, IL-15, and IL-18, which can induce the production of interferon-γ (IFN-γ) by natural killer (NK) cells. Mice treated with a combination of IL-15 and IL-12 developed gastrointestinal lesions, elevated acute-phase reactants, increased serum levels of proinflammatory cytokines, and apoptosis of NK cells [17]. Additionally, IL-15 has been found in several studies to regulate angiogenesis, with subcutaneous injection of IL-15 into nude mice continuously inducing angiogenesis in matrigel plugs [18]. Furthermore, Ad5-Ki67/IL-15 targeting glioma-associated mesenchymal stem cells (GA-MSCs) can reduce the expression of PD-L1 in glioma cells and neovascularization [19]. Nevertheless, the specific role of IL-15 in DR and its related molecular mechanisms has been rarely studied.

The signal transducer and activator of transcription (STAT) family plays a critical role in the complex network of intracellular signal transduction, activating its function in response to a variety of cytokines, such as IL-15, erythropoietin, growth hormone, and prolactin [20], especially the JAK/STAT signaling pathway. Johnston et al. [21] discovered that IL-2 and IL-15 could activate STAT5, transcriptional activator 3 (STAT3), and JAK. As a signaling pathway closely related to immune function, it not only participates in immune regulation but also plays a mediating role in the process of angiogenesis. For example, in vitro human models have shown that VEGF-activated STAT3 is crucial for the formation of tubular structures in endothelial cells [22], while the migration of endothelial cells induced by IL-3 is closely associated with the activation of STAT5 [23]. Additionally, platelet-rich plasma can promote angiogenesis by inhibiting the JAK/STAT signaling pathway, which is beneficial for the survival and repair of skin flaps [24]. In the context of non–small cell lung cancer, overexpression of PD-L1 promotes the production of angiogenic factors through the activation of the STAT signaling pathway, thereby stimulating angiogenesis and strengthening the formation of the tumor vascular system [25]. STAT5 is a member of the STAT family and is an important class of transcription factors. Studies have indicated that in DR, hypoxic conditions can activate the JAK2/STAT5 pathway, which plays a role downstream of VEGF to promote angiogenesis [26]. Furthermore, the activity of STAT5 is closely related to nuclear receptor coactivator 2 (NCOA2). In breast tissue, NCOA2 has been found to act as an important cofactor of STAT5 and regulate the transcriptional activity of STAT5 [27]. Although research has revealed the key role of JAK2/STAT5 in abnormal retinal neovascularization in DR, the specific molecular mechanisms of STAT5 in DR have not been fully explored. This study aims to fill this gap by deeply analyzing the molecular mechanisms of STAT5 in DR.

This research uses public databases for bioinformatics analysis, combined with clinical sample testing and in vitro experiments, to reveal the molecular mechanisms of the STAT5 signaling pathway induced by macrophage-secreted IL-15 in the pathogenesis of DR. It aims to provide new insights into the molecular mechanisms of DR and to develop new therapeutic strategies and treatment targets.

METHODS

Acquisition of public microarray data sets: This study used four microarray data sets from the Gene Expression Omnibus (GEO) database: GSE221521, GSE185011, GSE236333, and GSE179568. These data sets included blood and retinal tissue samples from healthy control groups, diabetic patients (DM group), and DR (DR group) patients. We downloaded the original count matrices (GSE236333 and GSE221521) and fragments per kilobase per million mapped fragments (FPKM) matrices (GSE185011 and GSE179568) and used R packages for data preprocessing, including background correction, normalization, and data filtering.

Initially, we obtained the original gene expression matrices from the GEO database for the following data sets: GSE221521, which includes blood samples from 50 healthy controls, 74 diabetic patients without retinopathy (DM group), and 69 DR (DR group) patients; GSE185011, containing peripheral blood mononuclear cell (PBMC) samples from 5 healthy controls and 5 patients with DR; GSE236333, studying the effects of the glucagon-like peptide 1 receptor agonist, liraglutide, on experimental DR in 6 healthy controls and 6 DR group retinal tissues; and GSE179568, including 7 retinal neovascularization (RNV) membranes (PDR), 10 macular puckers, and 7 macular holes samples. We used the R package limma function to analyze the differential gene sets between the DR group and the normal control group (Con) in the above data sets. We set a significant difference threshold of $|\log_2$ fold change$| > 0.5$ and $p < 0.05$ to screen for statistically significant differential genes.

Clinical sample collection: Human blood samples from 20 healthy individuals, 20 diabetic patients, and 20 patients with DR were collected from Hunan Children's Hospital and Xiangya Hospital of Central South University. The clinical information of the participants is shown in Table 1. The blood samples were centrifuged at 1006 ×g for 10 min at 4 °C. This study was conducted according to the principles of the Declaration of Helsinki. Our research obtained approval from the Ethics Committee of Hunan Children's Hospital after each patient signed an informed consent form.

Cell preparation and treatment: Human monocytic leukemia cells (THP-1) were purchased from the American Type Culture Collection (Manassas, VA). THP-1 cells have been identified by short tandem repeat (STR) analysis (Appendix 1) The process begins with the extraction of DNA from the cell sample, followed by a multiplex PCR amplification of multiple core STR loci using fluorescently labeled primers. The data are analyzed to determine the allele sizes and counts at each locus, producing a distinct STR profile. This profile is compared against reference databases (e.g., ATCC, DSMZ, JCRB, and RIKEN). STR analysis showed a match that confirms the cell line's authenticity (Appendix 2). Macrophages were divided into two groups and stimulated and cultured for 48 h with glucose solutions at concentrations of 5 nM (Con) and 25 nM (HG). The level of IL-15 in culture medium was detected using the human IL-15 ELISA Kit (ab218266; Abcam, Cambridge, UK).

Human retinal microvascular endothelial cells (hRMECs) and human umbilical vein endothelial cells (HUVECs) were purchased from the American Type Culture Collection. hRMECs and HUVECs have been identified by STR analysis and immunofluorescence using von Willebrand factor as a biomarker of vascular endothelial cells (Appendix 2). Cells were maintained in a mixture of DMEM (glucose-free, #11966025; Thermo Fisher Scientific, Waltham, MA) and Ham's F-12 Nutrient Mixture (10.0 mM d-glucose, #11765047; Thermo Fisher Scientific), containing normal-glucose concentrations (5 mM glucose, corresponding to normal human blood glucose levels), and were supplemented with 10% fetal bovine serum (FBS; Thermo Fisher Scientific) and 1% penicillin-streptomycin (P/S; Thermo Fisher Scientific) in a 37 °C, 5% CO_2 humidified incubator. hRMECs and HUVECs in the experimental group were cultured in medium containing high-glucose (HG) concentrations (25 mM glucose). In the coculture group, retinal endothelial cells were cocultured with THP-1 cells for 48 h.

Cell transfection: Small interfering RNAs (siRNAs) targeting STAT5, epithelial cell adhesion molecule 1 (EFNA1), and NCOA2 (siRNA-STAT5, siRNA-EFNA1, and siRNA-NCOA2) were synthesized by RiboBio (Guangzhou, China). The siRNA sequences are shown in Table 2. Before transfection, we prepared siRNAs at a working concentration (typically 50–100 nM) in transfection reagent (Lipofectamine

Table 1. Clinical information of the participants.

Clinical information	Normal	DM	DR
Number (n)	20	20	20
Gender (male/female)	10/10	11/9	11/9
Age (years)	69.34 ± 6.21	70.17 ± 7.16	71.64 ± 6.43
Body mass index	24.61 ± 2.33	23.83 ± 2.76	24.84 ± 3.17
Fasting blood glucose (mmol/l)	6.13 ± 1.42	8.47 ± 1.86	9.47 ± 2.07
Fasting insulin (μU/ml)	16.08 ± 4.68	15.18 ± 10.58	18.12 ± 9.56
Total cholesterol (mmol/l)	4.81 ± 2.54	4.70 ± 2.09	4.60 ± 2.48
Triglycerides (mmol/l)	1.66 ± 1.25	1.63 ± 1.42	1.80 ± 1.51
High-density lipoprotein cholesterol (mmol/l)	1.17 ± 0.45	1.05 ± 0.55	0.91 ± 0.38
Low-density lipoprotein cholesterol (mmol/l)	2.23 ± 1.22	2.65 ± 1.34	3.09 ± 1.56

Table 2. The sequences of the siRNAs.

Gene names	No.	Target seq (5′–3′)
	1	TCCGGCACATTCTGTACAATG
STAT5	2	GCGCTTTAGTGACTCAGAAAT
	3	CGCTTCTCTTTGGAAACAATA
	1	AGAGGTGCGGGTTCTACATAG
EFNA1	2	GTCTTCTGGAACAGTTCAAAT
	3	ACATCATCTGTCCGCACTATG
	1	ATCCGTTCTCAGACTACTAAT
NCOA2	2	CTTCGCTATTTGCTAGATAAA
	3	CCAGGAATGATGGGTAATCAA

2000; Invitrogen, Carlsbad, CA). siRNA transfection reagents were added to the growth medium of hRMECs and HUVECs before incubation for 24 to 48 h. The full length of human EFNA1 DNA was synthesized by Sangon Biotech and cloned into the pcDNA3.1 vector (Takara, Shiga, Japan) to construct overexpression plasmids pcDNA-EFNA1. DNA Midiprep Kits (Thermo Fisher Scientific) were used for preparing the overexpression plasmids. Cell transfections were performed using Lipofectamine 3000 (Invitrogen). Cells were harvested 48 h posttransfection to conduct further experiments.

IL-15 knockout cells: To generate IL-15 knockout THP-1 cells, we employed the CRISPR/Cas9 technology. The human monocytic cell line THP-1 was used for this purpose. Initially, we designed and synthesized a single guide RNA (sgRNA) sequence targeting a conserved region within the coding region of the IL-15 gene. The sgRNA sequence is as follows: 5′-GGA GAA TCC ATT CCA ATA TA TGG-3′. The sgRNA sequence was cloned into a plasmid vector containing the Cas9 expression cassette, provided by RiboBio, and the plasmid was used according to the manufacturer's instructions. For spCas9, the template for in vitro synthesis of guide RNA with T7 RNA polymerase can be prepared by annealing and primer extension of the following primers: IL15_guideRNA183fwT7crTarget: 5′-GAA ATT AAT ACG ACT CAC TAT AGG AGA ATC CAT TCC AAT ATA GTT TTA GAG CTA GAA ATA GCA AG-3′; IL15_guideRNAallT7common (constant primer used for all guide RNAs): 5′-AAA AGC ACC GAC TCG GTG CCA CTT TTT CAA GTT GAT AAC GGA CTA GCC TTA TTT TAA CTT GCT ATT TCT AGC TCT AAA AC-3′.

Following transfection of THP-1 cells with the CRISPR/Cas9 construct, knockout cells were selected using puromycin (2 µg/ml) for 7 days to enrich the population of successfully transfected cells. To generate a clonal cell line, the transfected pool was subsequently subjected to single-cell sorting by flow cytometry into 96-well plates. PCR and western blot assays were conducted to confirm the loss of IL-15 expression. The clone exhibiting complete IL-15 knockout was selected for subsequent experiments.

Flow cytometry assay: Human blood was collected into EDTA-treated tubes (Improve Medical, Guangzhou, China). PBMCs were isolated using Ficoll-Paque Plus density centrifugation (500g at room temperature without brake for 25 min). PBMCs were stained with phycoerythrin (PE)–conjugated anti-CD4 (1:100, #ab172730; Abcam), PE-conjugated anti-CD19 (1:400, #ab227688; Abcam), and PE-conjugated anti-CD163 (1:60, #ab182422; Abcam) antibodies at 4 °C for 1 h. The fluorescence of the stained cells was measured using a BD AccuriTM C6 cellometer (Becton, Dickinson, Franklin Lakes, NJ, USA). Data were analyzed with FlowJo software (Tree Star, Ashland, OR, USA).

RNA isolation and quantitative real-time PCR: Total RNA was extracted from the cells using TRIzol reagent (catalog number: 15,596,026; Invitrogen) and stored at −80 °C. After quantification of the RNA concentration with a NanoDrop 2000 spectrometer (Thermo Fisher Scientific), 1 µg total RNA was used to synthesize cDNA using a SureScript First-strand cDNA Synthesis Kit (QP057; GeneCopoeia, Guangzhou, China). A quantitative real-time PCR experiment was conducted with the QuantiTect Reverse Transcription kit (205,314; Qiagen, Hilden, Germany) in a 7500 Fast real-time PCR System (Thermo Fisher Scientific) under the following conditions: 94 °C for 10 min, followed by 40 cycles of 94 °C for 30 s, 60 °C for 30 s, and 72 °C for 40 s. Primer sequences are shown in Table 3. GAPDH was used as an internal control. Gene expressions were quantified with the $2^{-\Delta\Delta CT}$ method [28].

Western blot analysis: Total proteins were extracted with RIPA lysis buffer (Sigma-Aldrich, St. Louis, MO), and the protein concentration in each extract was determined using a BCA quantification kit (Beyotime, Shanghai, China). Next, an equal amount of protein from each extract was separated

by 12% sodium dodecyl sulfate–polyacrylamide gel electrophoresis, and the protein bands were transferred onto polyvinylidene fluoride membranes, which were subsequently blocked with 5% fat-free milk at room temperature for 2 h. Subsequently, the protein bands were probed with primary antibodies (Abcam) against IL-15 (1:200 dilution), p-STAT1 (1:200 dilution), STAT1 (1:200 dilution), p-STAT5 (1:200 dilution), STAT5 (1:200 dilution), EFNA1 (1:200 dilution), VEGF (1:500 dilution), p-AKT (1:500 dilution), p-AKT (1:500 dilution), p-Vav (1:200 dilution), NCOA2 (1:200 dilution), and β-actin (1:500 dilution) at 4 °C overnight, after which, the membranes were incubated with horseradish peroxidase–conjugated goat antirabbit secondary antibodies for 2 h at room temperature. The immunostained protein bands were detected with an enhanced chemiluminescence kit (Millipore, Burlington, MA). X-ray films were used for signal detection and quantification. To ensure the comparability of the western blot experimental results, all images were uniformly adjusted for brightness and contrast using Photoshop (Adobe, San Jose, CA) software.

Cell Counting Kit-8 assay: Cell viability was determined using the Cell Counting Kit-8 assay (CCK8; Dojindo, Kumamoto, Japan). Each assay was conducted in triplicate at 37 °C and using 10 µl of the CCK8 solution. The absorbance of each assay well at 450 nm was detected with a microplate reader. Proliferation rate (%) = [OD(Treatment) – OD(Control)] / OD(Control) * 100%.

5-Ethynyl-2′-deoxyuridine staining assay: Cells from different groups were cultured in 96-well plates for 24 h at 37 °C. The following day, the cells were incubated for 2 h with 50 µl 5-ethynyl-2′-deoxyuridine (EdU; Beyotime) solution at 37 °C and then fixed for 15 min with 4% paraformaldehyde at room temperature. Next, the cellular nuclei were stained with DAPI solution (Sigma-Aldrich), and images of EdU-positive cells were acquired under a microscope.

Wound-healing assay: A wound-healing assay was performed to assess cell migration capacity as follows: cells from different groups (5×10^5 cells/well) were seeded in a 6-well plate and starved for 24 h. Subsequently, cells were incubated with 10% FBS containing medium, and a plastic tip was used to create wounds across the cell monolayer. After 24 h, wound closure was photographed under an inverted microscope (magnification, ×100). The inhibitory rate was estimated according to the wound closure in each group.

Tube formation assay: Frozen vials of Matrigel membrane matrix (Thermo Fisher Scientific) were thawed on ice at +4 °C overnight. Matrigel was added (50 µl/well) into 96-well plates (TPP Techno Plastic Products AG, Trasadingen, Switzerland) and allowed to polymerize at 37 °C for 30 min. Meanwhile, cells were detached from wells/flasks using trypsin-EDTA (Gibco, Life Technologies, Carlsbad, CA). Using basal Vasculife medium (2% fetal bovine serum/FBS) with or without IL-6/sIL-6R (100 ng/ml each), suspension of cells was prepared, and 10^4 cells per well were added to the polymerized Matrigel in duplicate. The plates were placed in an IncuCyte S3 Live Cell Analyses System (Sartorius AG, Göttingen, Germany), and the tube formation progress was monitored over 24 h by taking pictures every hour (three images per well). The images (10× magnification) were subsequently analyzed using the Angiogenesis-Analyzer macro written for ImageJ (National Institutes of Health, Bethesda, MD).

Co-immunoprecipitation: The anti-STAT5, anti-NCOA2, and normal IgG were added to 1-mg cell lysates precleared with Protein G Agarose beads (Sigma-Aldrich) and then incubated at 4 °C overnight. The co-immunoprecipitation complexes were harvested and analyzed by western blot analysis.

Chromatin immunoprecipitation assay: The relationship between STAT5 protein and the EFNA1 promoter was determined by performing a chromatin immunoprecipitation assay with a chromatin immunoprecipitation (ChIP) assay kit

Table 3. The primer sequences.

Gene names	Direction	Sequence (5′–3′)	Tm
STAT1	Forward	CAGCTTGACTCAAAATTCCTGGA	60.7
	Reverse	TGAAGATTACGCTTGCTTTTCCT	60.5
STAT5	Forward	GCAGAGTCCGTGACAGAGG	61.7
	Reverse	CCACAGGTAGGGACAGAGTCT	62.1
EFNA1	Forward	TCAGGCCCATGACAATCCAC	61.9
	Reverse	GTGACCGATGCTATGTAGAACC	60.2
NCOA2	Forward	TGGGGCCTATGATGCTTGAG	61.4
	Reverse	GGTTTTTGACAAATTCCGTGTGG	60

(Upstate Biotechnology, Lake Placid, NY). In brief, the cells transfected with STAT5 or vector at 80% to 90% confluency were incubated for 15 h with 0.1 μg/ml doxycycline and cross-linked in 1% formaldehyde. After sonication, the precleaned supernatants were incubated with streptavidin-coated magnetic beads conjugated with human anti-STAT5 or anti-IgG antibody (Sigma-Aldrich) for 20 min. The beads were washed, digested with proteinase K, and used for extracting eluted DNA. Next, the enrichment of EFNA1 was analyzed via PCR for the ChIP assay.

Statistical analysis: All statistical data were analyzed using GraphPad Prism 8 software (GraphPad Prism, La Jolla, CA), and quantitative data are presented as the mean ± standard deviation. Comparisons between two groups were performed using the Student *t* test, and comparisons between multiple groups were performed by one-way analysis of variance, followed by Dunnett's post hoc test. A p value <0.05 was considered statistically significant.

RESULT

PBMCs may influence gene expression in the retinal tissues of patients with DR: We employed the DR-related data sets GSE236333 and GSE179568 for an intersection analysis. This analysis led to the identification of 72 genes that were upregulated in the retinal tissues across both data sets. In a similar manner, we performed an intersection analysis using the data sets GSE185011 and GSE221521 to screen for upregulated genes in the blood and PBMCs of patients with DR (Figure 1A, B). A total of 27 upregulated genes were found within the intersection area. To investigate whether the upregulated genes in the blood and PBMCs of patients with DR affect gene expression in retinal tissues, we constructed a protein-protein interaction network of these differentially expressed genes. This was achieved by using the STRING database in conjunction with the CytoNCA plugin in Cytoscape. The results demonstrated that three genes (ATM, IL15, and CD36) in peripheral blood samples exhibited the strongest associations with the most upregulated genes in the retinal tissues. These included the five most significantly upregulated genes: STAT1, CD274, STAT5A, TMP1, and FN1 (Figure 1C). Notably, STAT1 and STAT5A are well recognized as transcription factors. Through predictions from the CHEA and ENCODE databases, we discovered that SBNO2 and EFNA1 might serve as their downstream target genes (Figure 1D). Moreover, both of these genes were upregulated in the retinal tissues of patients with DR. Gene functional enrichment analysis (GO-BP) revealed that the 72 upregulated genes in the retinal tissues of patients with DR were associated with various biological processes, including cytokine production, angiogenesis, wound healing, and immune responses (Figure 1E). We also presented the expression levels of STAT5A, EFNA1, and STAT1 in data sets GSE236333 and GSE179568 (Figure 1F, H), as well as the expression of IL-15 in data sets GSE185011 and GSE221521 (Figure 1G, I). Collectively, we hypothesized that upregulated genes, such as IL-15, in the blood and PBMCs of patients with DR influence the expression of genes such as STAT5A and STAT1 in retinal tissues. Subsequently, STAT5A and STAT1 induce the expression of EFNA1, which may be involved in certain pathological processes of DR.

Elevated expression of EFNA1 in retinal endothelial cells: This study analyzed a single-cell RNA sequencing data set, GSE245561, of patients with DR. Within the retinal fibrovascular membrane tissues, we successfully identified five distinct cell types: endothelial cells, T cells, stromal cells, macrophages, and epithelial cells (Figure 2A, B). Notably, we observed that the EFNA1 gene exhibited a high level of expression in endothelial cells (Figure 2C, D). To further elucidate the role of EFNA1 in endothelial cells, we partitioned the endothelial cells into two primary groups: a negative group consisting of 653 cells without EFNA1 expression and a positive group comprising 1,075 cells with EFNA1 expression (Figure 2E, F). Subsequently, based on the median expression level of EFNA1, we subdivided the positive group into low and high EFNA1 expression subgroups (Figure 2E, F). By applying the FindMarkers algorithm for differential gene analysis between these groups, we established a threshold for screening differential genes. The analysis revealed that between the high and low EFNA1 expression groups, there were 90 downregulated genes, 1,572 genes with stable expression, and 76 upregulated genes (Figure 2G). We then presented the top five genes (*CXCR4*, *NCOA2*, *INHBB*, *EFNB2*, and *SAT1*) in the high EFNA1 expression group and the top five genes (*CDH11*, *DLC1*, *ACTN1*, *NR2F2*, and *PRCP*) in the low EFNA1 expression group (Figure 2H, I). The expression of these genes was closely correlated with the expression of EFNA1 (Figure 2I), suggesting that these genes are under the regulatory control of EFNA1.

HG induced the expression of IL-15 in macrophages: In this study, we collected blood samples from healthy individuals, diabetic patients, and patients with DR and isolated PBMCs from them. IL-15 expression levels were significantly higher in PBMCs from patients with DR than in normal diabetic patients and healthy individuals (Figure 3A, B). PBMCs refer to cells with a single nucleus and mainly include lymphocytes and monocytes/macrophages. Lymphocytes are divided into T and B lymphocytes. To determine which cell type had the most pronounced IL-15 upregulation in patients with DR,

we flow-sorted PBMCs (Figure 3C) and measured IL-15 mRNA expression levels in the three cell types (Figure 3D). Lymphocyte marker CD4, pan-B lymphocyte marker CD19, and monocytes/macrophages marker CD163 all had

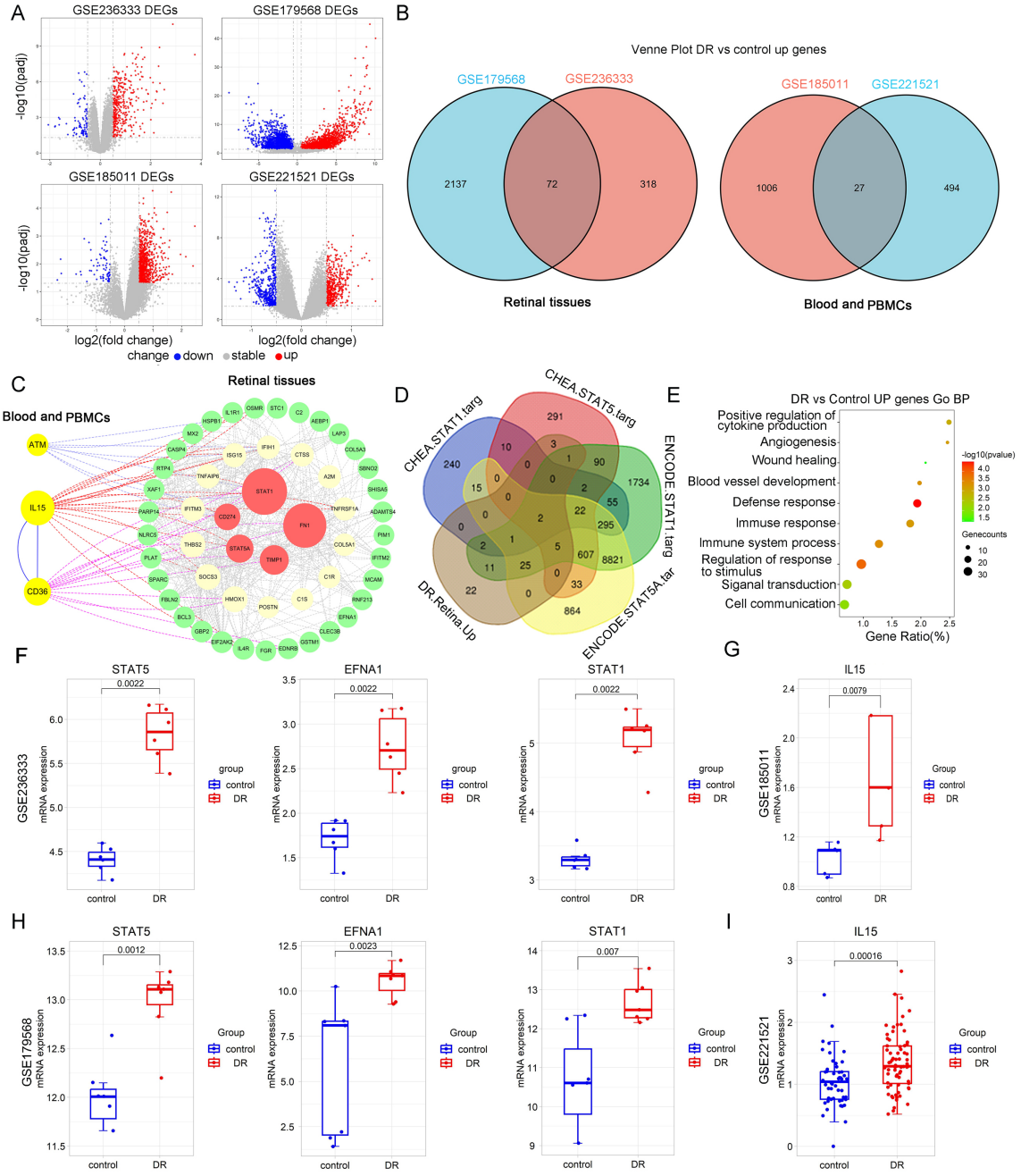

Figure 1. Differential gene expression analysis. **A**. Volcano plot of upregulated genes in the data sets GSE236333, GSE179568, GSE185011, and GSE221521. **B**. Venn diagram of gene intersection analysis between GSE236333 and GSE179568, as well as between GSE185011 and GSE221521. **C**. The highly expressed genes (72+27) in DR retinal tissue and peripheral blood samples were imported into the STRING database, and a network of moderately associated genes (interaction score >0.4) was selected. The highly related genes were further selected using the betweenness centrality method in Cytoscape with the CytoNCA plugin package. **D**. Downstream target genes were predicted using the CHEA and ENCODE databases, and an intersection analysis was performed with the 72 upregulated genes in DR retinal tissue. **E**. Gene Ontology enrichment analysis of the 72 upregulated genes in DR retinal tissue. **F–I**. Expression differences of STAT5A, EFNA1, STAT1, and IL-15 between two groups.

enrichment levels above 90%, with monocytes/macrophages having the highest levels of IL-15. A monocyte/macrophage cell line (THP-1) was used in the study in vitro. THP-1 cells were treated with different concentrations of glucose solution, and the expression level of IL-15 was detected. There was a significant difference in the expression level of IL-15 between the cells treated with 5-nM and 25-nM concentrations (Figure 3E). THP-1 cells were stimulated with 5-nM and 25-nM concentrations of glucose solution. By western blot and the enzyme-linked immunosorbent assay, we found that HG stimulation significantly increased the production and secretion of IL-15 of THP-1 cells, consistent with clinical studies showing that IL-15 expression was elevated in monocytes/macrophages from patients with DR (Figure 3F, G).

IL-15 promotes the proliferation, migration, and angiogenesis of retinal vascular endothelial cells and interacts with the HG environment: To evaluate the effect of IL-15 on the function of retinal vascular endothelial cells (hRMECs and HUVECs) in an HG environment, we assessed the impact of

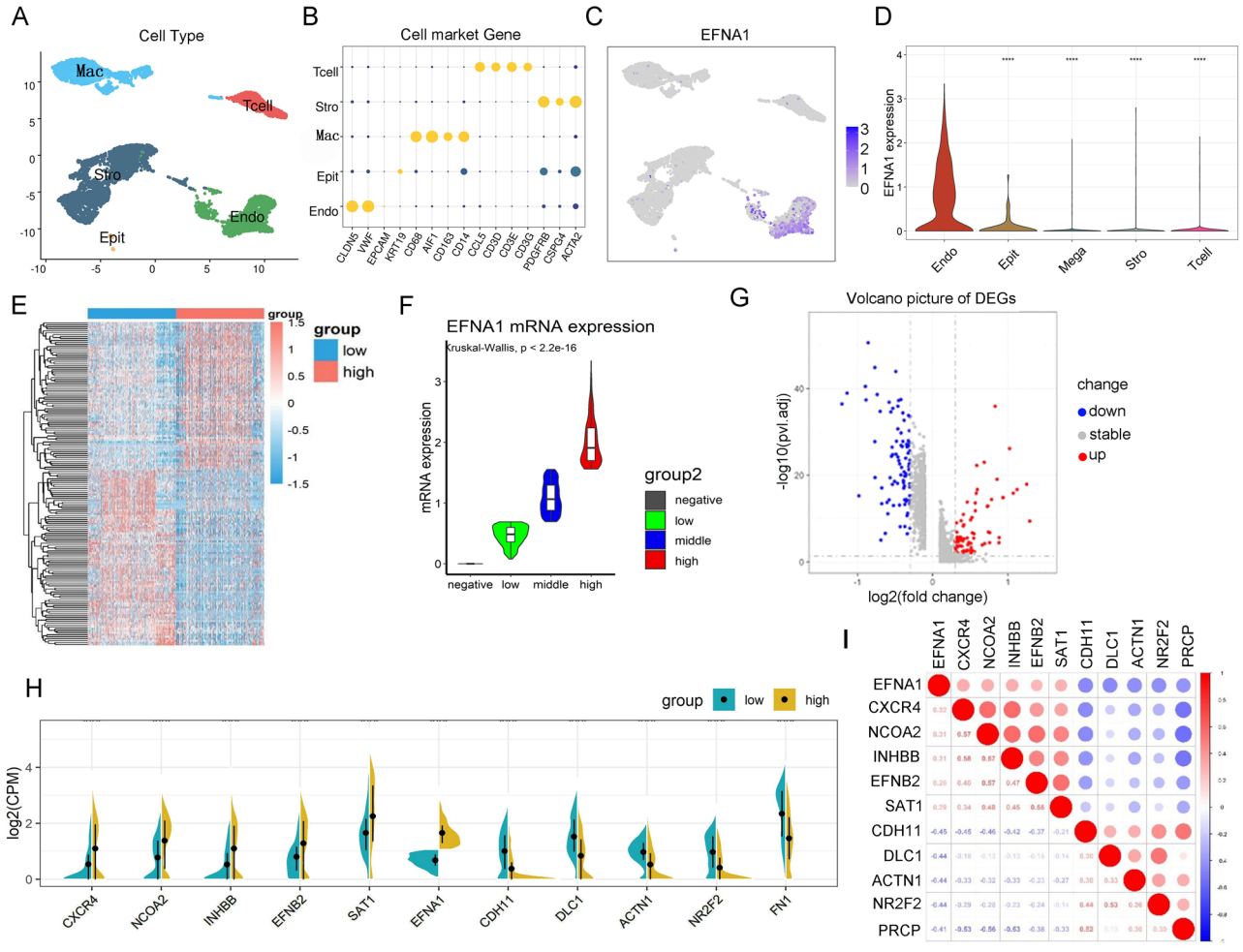

Figure 2. Cell cluster identification and related gene screening. **A**. Uniform manifold approximation and projection (UMAP) plot representing the five cell types identified through the analysis of single-cell RNA-seq data from four DR tissue samples in the GSE245561 data set, with data preprocessing following the literature method (nFeature_RNA >500; percent_mito <25) for clustering identification. **B**. Dot plot of common cell-specific markers. **C**. UMAP plot of EFNA1 expression across the five cell types. **D**. Violin plot of EFNA1 expression across the five cell types. **E**. Heatmaps of differentially expressed genes between high and low EFNA1 expression groups. FindMarkers were used for intergroup differential gene analysis, and thresholds were set to screen for differentially expressed genes, including a minimum percentage threshold of >0.3 in both groups, an absolute value of average $\log_2$ fold change of >0.3, and a *p* value of <0.01. **F**. The violin chart was divided into four groups according to the expression level of EFNA1. The horizontal bars in the box represent the median. The top and bottom of the box represent the 25th and 75th percentiles, and the lines extend into a 1.5× quartile range. **G**. Gene volcano map of EFNA1 low expression group and EFNA1 high expression group. **H, I**. Correlation analysis of significantly differentially expressed genes with EFNA1 was performed to screen out the top five genes with positive and negative correlation ≥0.3 and *p* value <0.05 with EFNA1.

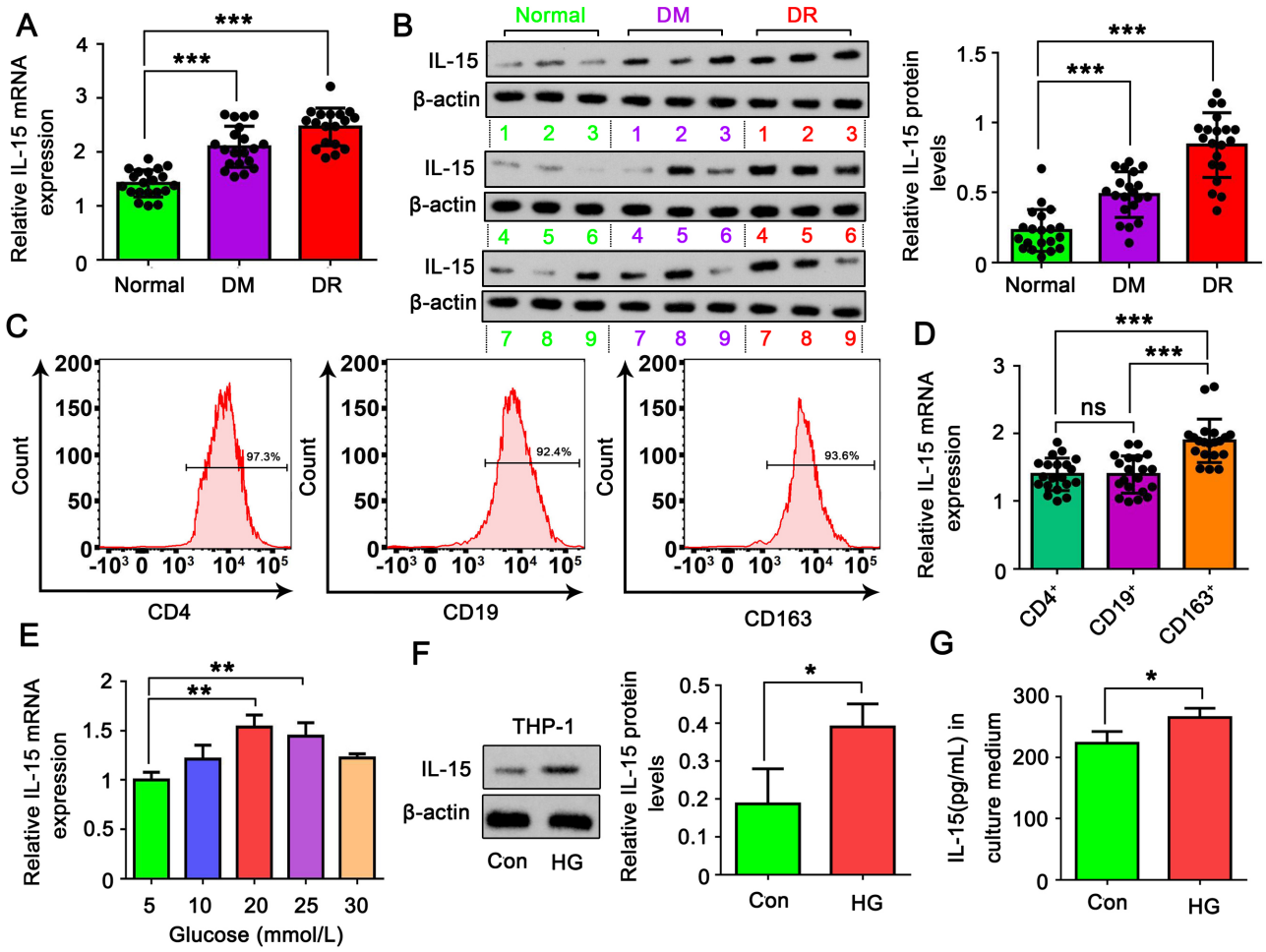

Figure 3. High expression of IL-15 in DR. **A**. The expression of IL-15 in blood PBMCs was detected by quantitative real-time PCR (n = 20). B. The expression of IL-15 in blood PBMCs was detected by western blot assay (n = 20). The western blot pictures show nine representative samples in each group. C. The enrichment levels of T lymphocyte marker CD4, pan-B lymphocyte marker CD19, and monocyte/macrophage marker CD163 were quantitatively detected by flow cytometry. The number represents a percentage of the total cell count. **D**. Quantitative real-time PCR was used to detect IL-15 mRNA expression levels of three kinds of cells in PBMCs in patients with DR (n = 20). **E**. A cell line of monocytes/macrophages (THP-1) was used in this study in vitro. THP-1 cells were treated with 5, 10, 20, 25, and 30 mmol/l glucose solution, and IL-15 mRNA expression levels were detected by quantitative real-time PCR (n = 3). **F, G**. THP-1 cells were stimulated with 5 nM (Con) and 25 nM (HG) glucose solutions, and IL-15 expression levels were detected by western blot and enzyme-linked immunosorbent assay (n = 3). *$p < 0.05$, **$p < 0.01$, ***$p < 0.001$. Statistical significance was determined by using an unpaired Student *t* test for two groups or one-way analysis of variance for more than two groups. Subsequently, Dunnett's post hoc tests were conducted. $p < 0.05$ was considered significant.

different concentrations of IL-15 (0, 10, 50, 200, 1,000 nM) at different time points (0, 12, 24, 48 h) on endothelial cell viability using the CCK8 assay. The results showed that when treated with 200 nM IL-15 for 48 h, cell viability reached the highest level, so this condition was used for subsequent experiments (Figure 4A). Subsequently, we treated hRMECs and HUVECs with 25 nM glucose solution and 200 nM IL-15. The results showed an increase in cell proliferation after 48 h of treatment with IL-15 alone or HG and a further increase after combined treatment of the two (Figure 4B, C). The wound-healing assay revealed an increase in the migration capacity of hRMECs and HUVECs after treatment with IL-15 alone or HG and a further increase after combined treatment with IL-15 and HG (Figure 4D). To determine the effect of combined IL-15 and HG treatment on endothelial cell angiogenesis, we examined the ability of cells in each group to form tubes. The results showed that the tube formation ability of hRMECs and HUVECs was improved after treatment with IL-15 or HG alone, and it further improved after combined treatment of the two (Figure 4E). Moreover, treatment with

IL-15 alone or in combination with HG significantly increased the mRNA expression levels of STAT1, STAT5, and EFNA1 in hRMECs and HUVECs (Figure 4F). With β-actin as the internal control, p-STAT1, STAT1, p-STAT5, STAT5, and EFNA1 protein levels were increased by IL-15 in hRMECs and HUVECs. HG increased STAT1 and EFNA1 but had a minor effect on the p-STAT1, p-STAT5, and STAT5 protein levels. Interestingly, cotreatment with IL-15 and HG exerted a stronger promoting effect on the protein levels of p-STAT1, STAT1, p-STAT5, STAT5, and EFNA1 than treatment with IL-15 alone. The results suggest that the effect of IL-15 on endothelial cells was more pronounced under HG conditions (Figure 4F, G). In conclusion, IL-15 promotes the proliferation, migration, and angiogenic capacity of retinal vascular endothelial cells, and an HG environment exacerbates these effects of IL-15.

MDM-secreted IL-15 promotes the proliferation, migration, and angiogenesis of vascular endothelial cells under HG conditions: To further investigate the effect of macrophage-secreted IL-15 on the function of hRMECs and HUVECs under HG conditions, we stimulated vascular endothelial cells and THP-1, a type of monocyte/macrophage (MDM), with HG solution separately, knocked out the *IL-15* gene in HG-treated THP-1, and then cocultured the two cells. The knockout of the *IL-15* gene in THP-1 was validated by PCR and western blot tests (Appendix 2). The experiment was divided into five groups: control group (Con), endothelial cells cocultured with THP-1 (MDM) group, endothelial cells cocultured with HG-stimulated THP-1 (HG MDM) group, endothelial cells cocultured with HG-stimulated THP-1 with IL-15 knockout (HG MDM–IL-15 KO) group, and endothelial cells treated with HG and cocultured with HG-stimulated THP-1 (HG + HG MDM) group. CCK8 and EdU staining results showed that after 48 h of coculture, endothelial cell proliferation did not change significantly in the MDM group, whereas endothelial cell proliferation in the HG MDM group was significantly increased. After IL-15 knockout, this increase was significantly reversed, suggesting that HG-stimulated macrophages promote endothelial cell proliferation by secreting IL-15. Compared to the HG MDM group, the proliferation ability in the HG + HG MDM group was also significantly increased, indicating that the HG environment of endothelial cells could promote cell proliferation (Figure 5A, B). In addition, the migration rate of endothelial cells was increased in the HG MDM group compared with the Con group, and this increase was significantly inhibited by IL-15 knockout. Endothelial cell migration was more pronounced in the HG + HG MDM group than in the HG MDM group (Figure 5C). The enhanced angiogenic ability of HG MDMs was reversed after IL-15 knockout. The angiogenic capacity of endothelial cells in HG + HG MDMs was also higher than that in the HG MDM group (Figure 5D). The levels of p-STAT1, STAT1, p-STAT5, STAT5, and EFNA1 were significantly increased in endothelial cells after coculture with HG-stimulated THP-1 cells, especially for STAT5, which showed the most significant increase. Knockout of IL-15 in HG-stimulated THP-1 markedly reversed the high expression of p-STAT1, STAT1, p-STAT5, STAT5, and EFNA1 in endothelial cells (Figure 5E, F). Overall, our experimental results indicate that macrophage-secreted IL-15 plays a key regulatory role in endothelial cell function under HG conditions. The absence of IL-15 can significantly reverse the enhancement of endothelial cell proliferation, migration, and angiogenesis induced by HG-stimulated macrophages.

Interference with STAT5 inhibits IL-15–induced EFNA1 expression, inhibiting the proliferation, migration, and angiogenesis of retinal vascular endothelial cells: To understand the effect of the STAT5/EFNA1 signaling axis on endothelial cell function, we treated hRMECs and HUVECs with IL-15 and transfected siRNA-STAT5 to knock down STAT5 expression. This study designed three siRNAs to knock down STAT5. The PCR test showed that siRNA1 had the highest efficiency to downregulate STAT5. siRNA1 was used in the following study for STAT5 knockdown (Appendix 2). After 48 h of culture under normal glucose conditions, we found that IL-15 treatment significantly increased the protein expression levels of p-STAT5, STAT5, and EFNA1 in hRMECs and HUVECs. After knocking down STAT5 expression, the increase in p-STAT5 and EFNA1 expression induced by IL-15 was significantly reversed (Figure 6A). As indicated by CCK8 testing, IL-15 treatment significantly improved the proliferation ability of hRMECs and HUVECs. After STAT5 expression was knocked down, the increase in endothelial cell proliferation induced by IL-15 was reversed (Figure 6B). Knockdown of STAT5 alone had a moderate effect on the viability of endothelial cells. EdU staining experiments showed consistent results from CCK8 testing (Figure 6C). In terms of cell migration ability, IL-15 treatment significantly promoted the migration of hRMECs and HUVECs, and the enhancement of migration ability was significantly reversed after STAT5 knockdown (Figure 6D, E). Finally, the angiogenesis experiment showed that IL-15 treatment enhanced the angiogenic ability of hRMECs and HUVECs, but this enhancement was significantly reversed after STAT5 knockdown, indicating that IL-15 regulates angiogenesis through the STAT5 pathway (Figure 6F). In summary, IL-15 promotes the proliferation, migration, and angiogenesis of retinal vascular endothelial cells by upregulating STAT5 protein.

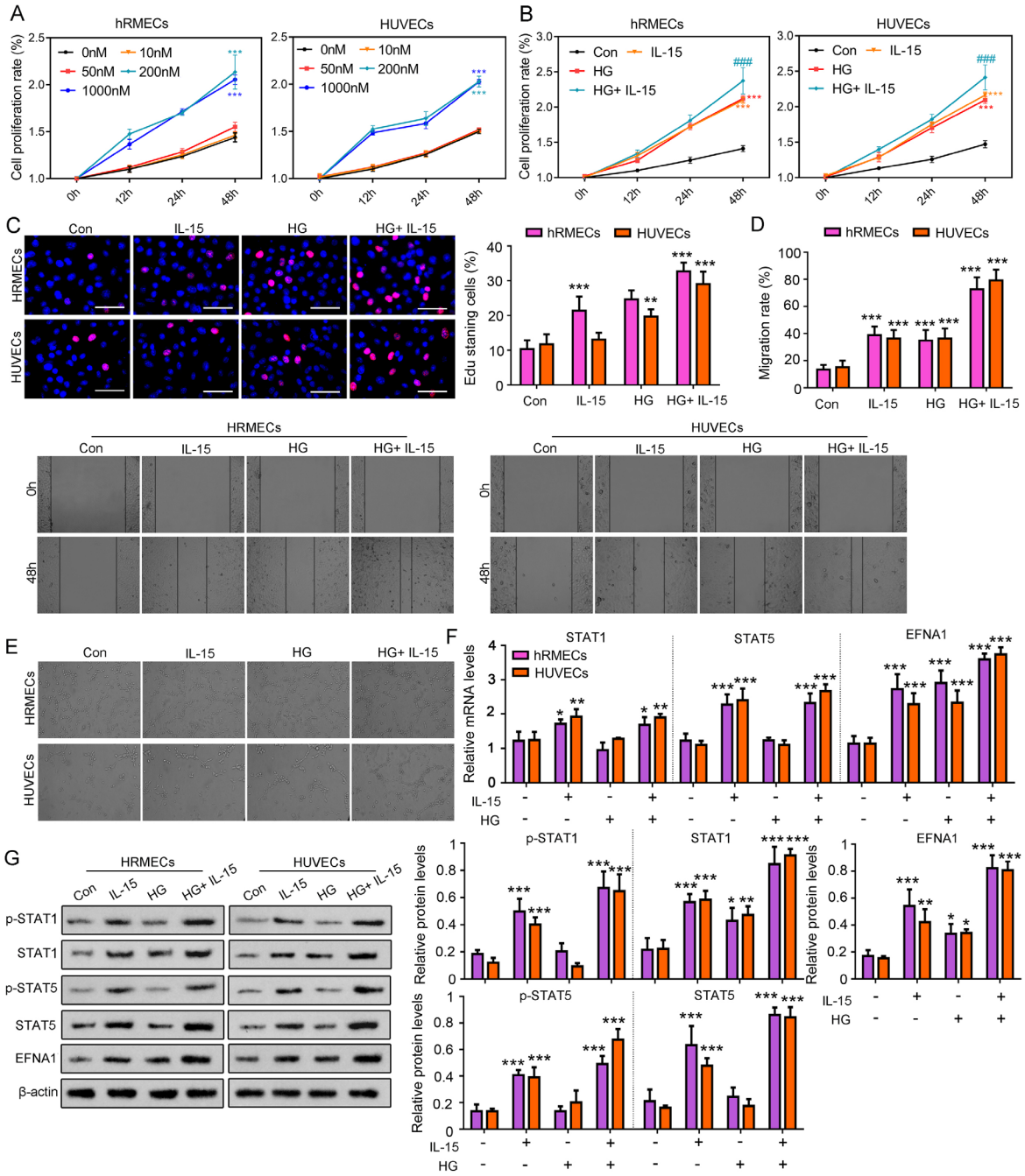

Figure 4. IL-15 promotes the proliferation, migration, and angiogenesis of retinal vascular endothelial cells and interacts with the HG environment. **A**. The CCK8 assay was used to evaluate the cell viability of vascular endothelial cells (hRMECs and HUVECs) at different concentrations of IL-15 (0, 10, 50, 200, 1,000 nM) at different time points (0, 12, 24, 48 h). **B**. hRMECs and HUVECs were treated with 25 nM glucose (HG) and 200 nM IL-15, alone or in combination. The CCK8 assay was conducted to detect the cell proliferation rate of vascular endothelial cells cultured for 0, 12, 24, and 48 h. **C**. EdU staining was used to assess cell proliferation ability. **D**. The cell wound-healing assay was used to detect cell migration ability. **E**. The angiogenesis assay was used to detect tubule formation ability. **F**. The mRNA expression levels of STAT1, STAT5, and EFNA1 were detected by quantitative real-time PCR. **G**. The protein levels of p-STAT1, STAT1, p-STAT5, STAT5, and EFNA1 were detected by western blot. *$p < 0.05$, **$p < 0.01$, ***$p < 0.001$ versus Con. #$p < 0.05$, ##$p < 0.01$, ###$p < 0.001$ versus HG. n = 3. Statistical significance was determined by using one-way analysis of variance for more than two groups. Subsequently, Dunnett's post hoc tests were conducted. $p < 0.05$ was considered significant.

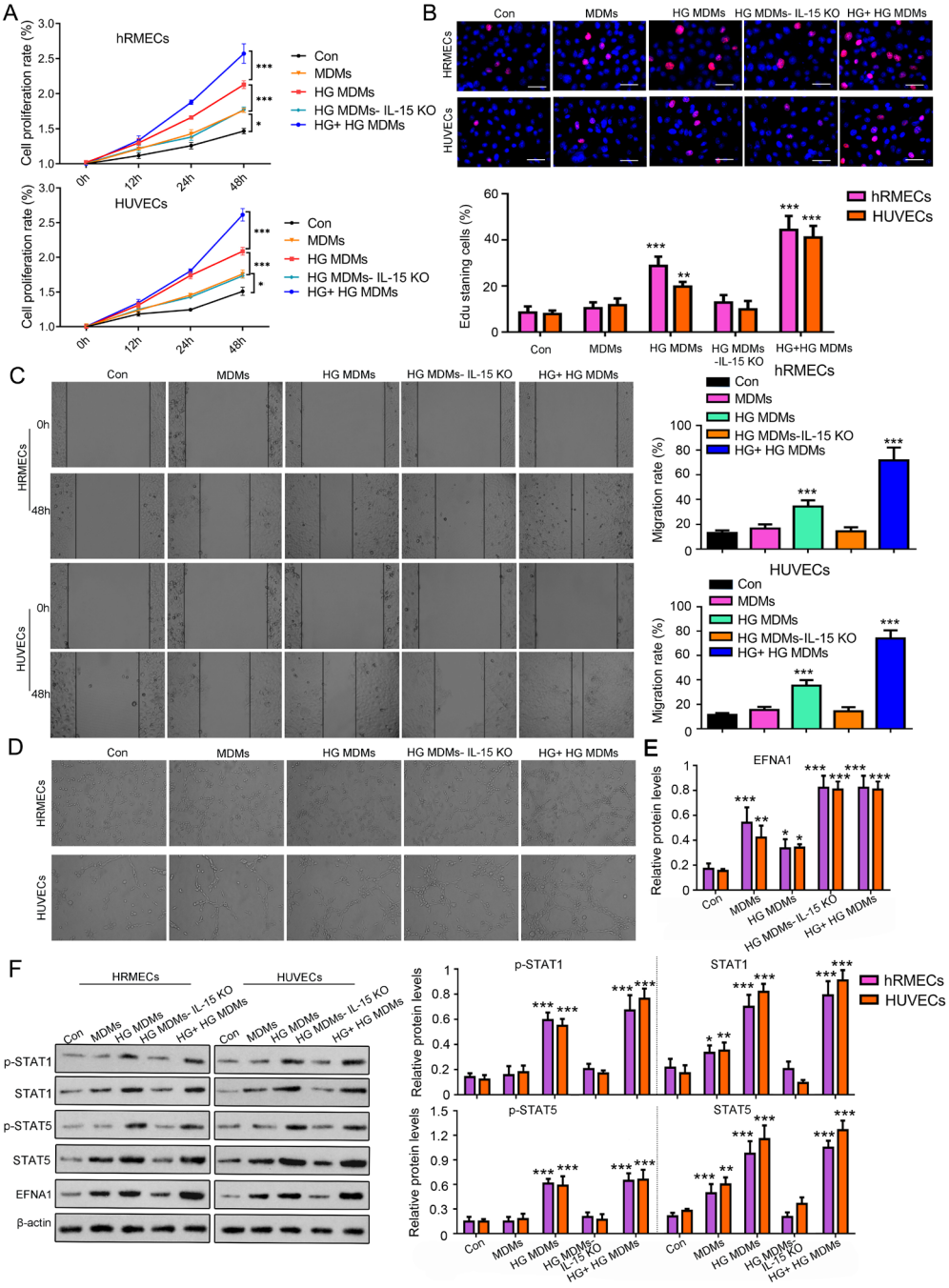

Figure 5. MDM-secreted IL-15 promotes the proliferation, migration, and angiogenesis of vascular endothelial cells under HG conditions. The experiment was divided into five groups: control group (Con), endothelial cells cocultured with THP-1 (MDM) group, endothelial cells cocultured with HG-stimulated THP-1 (HG MDM) group, endothelial cells cocultured with HG-stimulated THP-1 with IL-15 knockout (HG MDM–IL-15 KO) group, and endothelial cells treated with HG and cocultured with HG-stimulated THP-1 (HG + HG MDM) group. Vascular endothelial cells and THP-1 were stimulated with HG solutions (25 nM glucose), and the IL-15 gene was knocked out in THP-1 treated with HG. The two types of cells were then cocultured. **A**. The CCK8 assay was used to detect the cell proliferation rate of vascular endothelial cells cultured for 0, 12, 24, and 48 h. **B**. EdU staining was used to assess cell proliferation ability. **C**. The cell wound-healing assay was used to detect cell migration ability. **D**. The angiogenesis assay was used to detect tubule formation ability. **E, F**. Western blot was used to detect the protein expression levels of p-STAT1, STAT1, p-STAT5, STAT5, and EFNA1. *$p < 0.05$, **$p < 0.01$, ***$p < 0.001$. n = 3. Statistical significance was determined by using an unpaired Student *t* test for two groups or one-way analysis of variance for more than two groups. Subsequently, Dunnett's post hoc tests were conducted. $p < 0.05$ was considered significant.

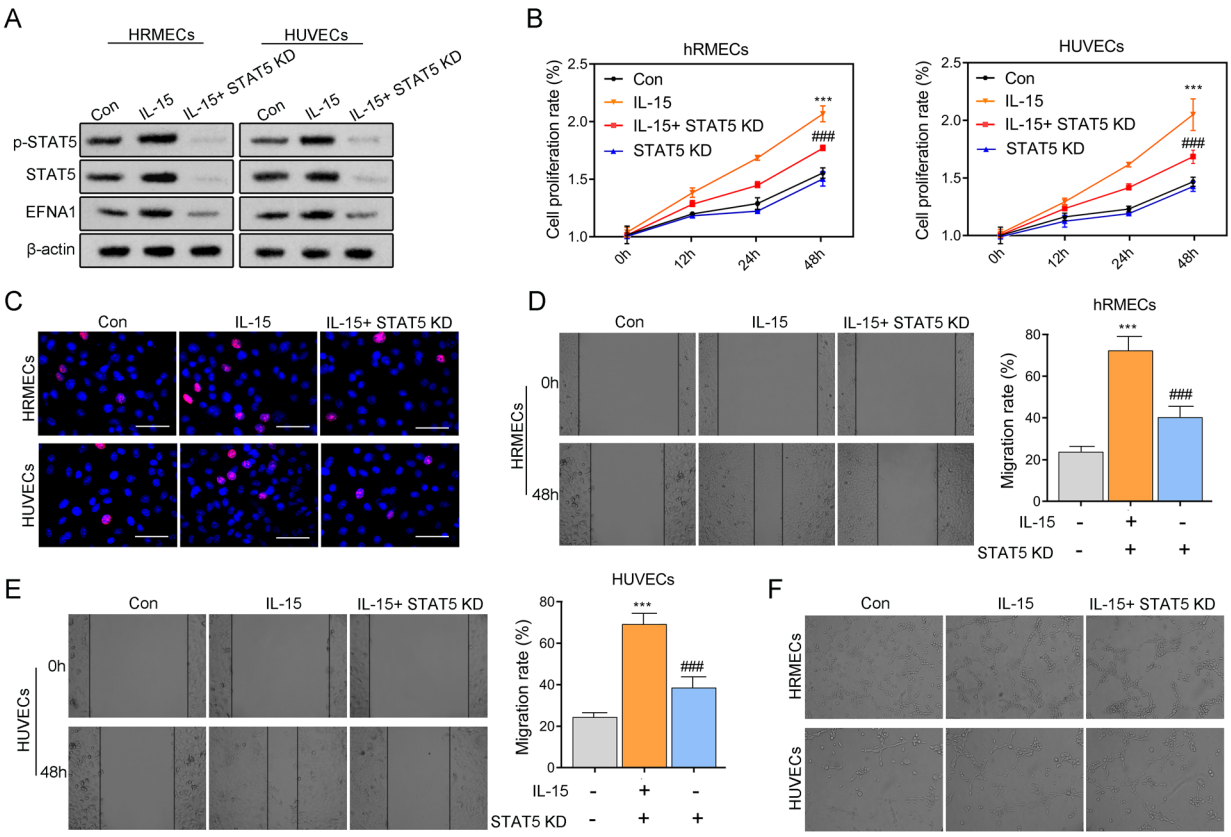

Figure 6. Interference with STAT5 inhibits IL-15–induced EFNA1 expression, inhibiting the proliferation, migration, and angiogenesis of retinal vascular endothelial cells. **A**. hRMECs and HUVECs were treated with IL-15 and transfected with siRNA-STAT5 to knock down STAT5 expression and then cultured for 48 h under normal glucose concentration. Western blot experiment was used to detect the protein expression levels of p-STAT5, STAT5, and EFNA1. **B**. CCK8 was used to detect the cell proliferation rate of vascular endothelial cells cultured for 0, 12, 24, and 48 h. **C**. EdU staining was used to assess cell proliferation ability. **D, E**. The cell wound-healing assay was used to detect cell migration ability. **F**. The angiogenesis assay was used to detect tubule formation ability. *$p < 0.05$, **$p < 0.01$, ***$p < 0.001$ versus Con. #$p < 0.05$, ##$p < 0.01$, ###$p < 0.001$ versus IL-15. n = 3. Statistical significance was determined by using one-way analysis of variance for more than two groups. Subsequently, Dunnett's post hoc tests were conducted. $p < 0.05$ was considered significant.

HG and IL-15 promote the proliferation, migration, and angiogenesis of retinal vascular endothelial cells by the upregulation of EFNA1: As a downstream target of STAT5, EFNA1 has been shown to promote angiogenesis through interacting with molecules such as Vav and AKT. To further validate the role and mechanism of EFNA1 in DR, we treated hRMECs and HUVECs with HG stimulation and IL-15 and transfected them with siRNA-EFNA1. This study also designed three siRNAs to knock down EFNA1. The PCR test showed that siRNA1 had the highest efficiency to down-regulate EFNA1. siRNA1 was used in the following study for EFNA1 knockdown (Appendix 2). After HG stimulation and IL-15 treatment, we found that the phosphorylation levels of AKT and Vav in hRMECs and HUVECs cells were significantly increased, and this increase in phosphorylation levels induced by HG and IL-15 was significantly reversed after EFNA1 expression was knocked down (Figure 7A). CCK8 and EdU staining experiments showed that HG and IL-15 treatment significantly improved the cell proliferation ability of hRMECs and HUVECs. However, when EFNA1 expression was knocked down, the increase in cell proliferation ability induced by HG and IL-15 was significantly inhibited (Figure 7B, C). The cell wound-healing assay indicated that HG and IL-15 treatment significantly promoted the migration ability of hRMECs and HUVECs, and this enhancement in migration ability was significantly reversed after EFNA1 knockdown (Figure 7D, E). Finally, the angiogenesis experiment showed that HG and IL-15 treatment significantly improved the tubule formation ability of hRMECs and HUVECs, and this enhancement in angiogenesis induced by HG and IL-15 was reversed after EFNA1 knockdown (Figure 7F). In summary, our experimental results indicate that IL-15 and

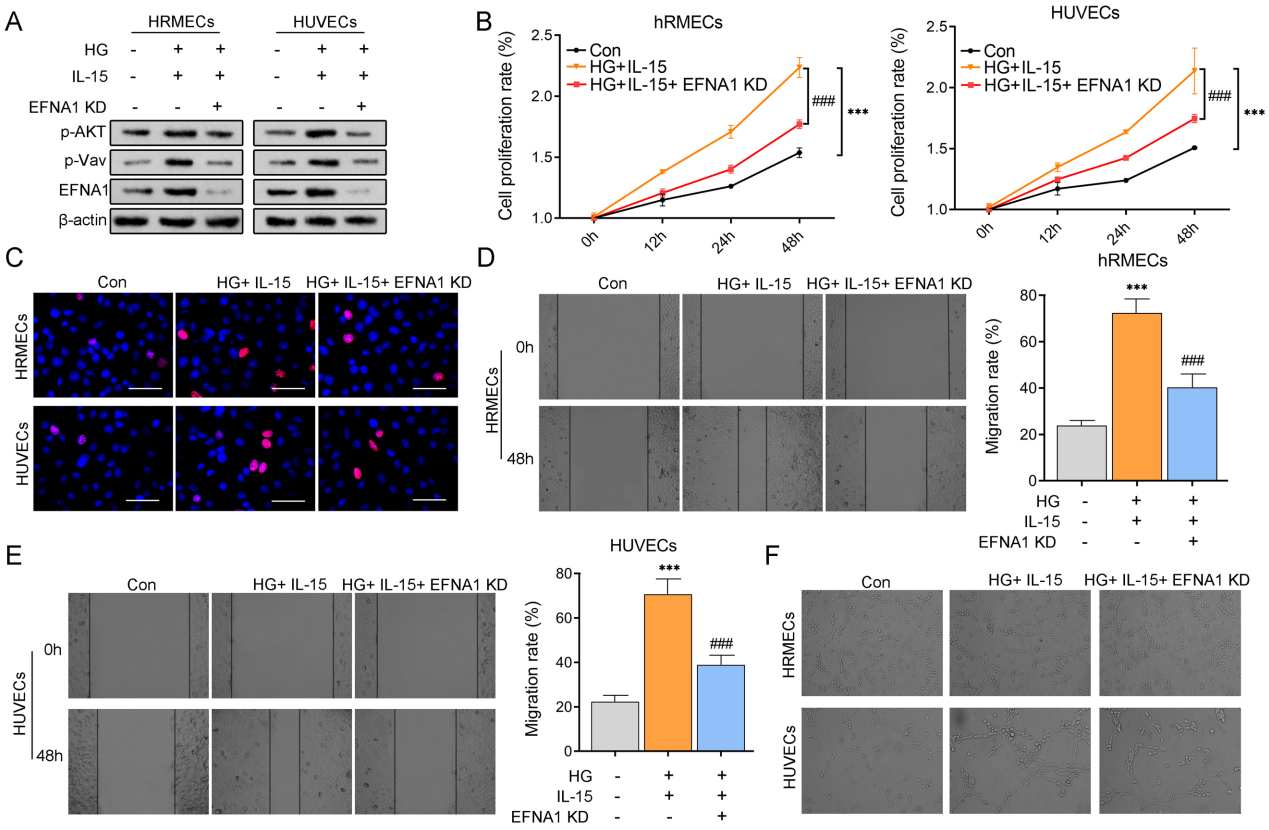

Figure 7. HG and IL-15 promote the proliferation, migration, and angiogenesis of retinal vascular endothelial cells by mediating the upregulation of EFNA1. **A**. hRMECs and HUVECs were stimulated with HG, overexpressed with IL-15, and then transfected with siRNA-EFNA1. WB was used to detect the protein expression levels of p-AKT, p-Vav, and EFNA1. **B**. CCK8 was used to detect the cell proliferation rate of vascular endothelial cells cultured for 0, 12, 24, and 48 h. **C**. EdU staining was used to assess cell proliferation ability. **D, E**. The cell wound-healing assay was used to detect cell migration ability. **F**. The angiogenesis assay was used to detect tubule formation ability. *$p < 0.05$,**$p < 0.01$,***$p < 0.001$ versus Con. #$p < 0.05$, ##$p < 0.01$, ###$p < 0.001$ versus HG+IL-15. n = 3. Statistical significance was determined by using one-way analysis of variance for more than two groups. Subsequently, Dunnett's post hoc tests were conducted. $p < 0.05$ was considered significant.

HG promote the proliferation, migration, and angiogenesis of retinal vascular endothelial cells by upregulating EFNA1 expression. These findings further reveal the importance of the IL-15/EFNA1 pathway in DR and provide new potential targets for the treatment of vascular complications in DR.

NCOA2 as a transcriptional coactivator induces positive feedback regulation of STAT5/EFNA1: In Figure 2H, I, we screened the top 10 genes. Their expression was most closely correlated with EFNA1 expression. For example, a higher expression of NCOA2 was observed in the high-EFNA1-expression group, while a lower expression of NCOA2 was observed in the low-EFNA1-expression group. This suggested that NCOA2 expression was influenced by EFNA1. NCOA2 is a transcriptional coactivator that can enhance the binding efficiency of transcription factors to DNA, thereby synergistically regulating gene expression. We hypothesized that NCOA2 can conversely influence EFNA1 expression by acting as a transcriptional coactivator of some transcription factors, such as STAT5. To understand the mutual relationship between EFNA1 and NCOA2, we overexpressed EFNA1 and knocked down NCOA2 in hRMECs and HUVECs. Three siRNAs have been designed to knock down NCOA2. The PCR test showed that siRNA2 had the highest efficiency to downregulate NCOA2. siRNA2 was used in the following study for NCOA2 knockdown (Appendix 2). The PCR and western blot results showed that EFNA1 overexpression increased not only EFNA1 but also NCOA2 in hRMECs and HUVECs. After transfecting siRNA-NCOA2, the expression of both EFNA1 and NCOA2 in the cells was decreased. NCOA2 knockdown also reversed the increase in EFNA1 and NCOA2 expression in cells with EFNA1 overexpression. These results suggest a mutually promoting effect of EFNA1 and NCOA2 (Figure 8A,

B). This study also knocked down NCOA2 in IL-15–treated endothelial cells. IL-15 increased the expression of EFNA1 in the cells. Knocking down NCOA2 partially reversed an IL-15–induced increase in EFNA1 expression (Figure 8C). A co-immunoprecipitation experiment showed that IL-15 treatment significantly increased the interaction between STAT5 and NCOA2, and this interaction was significantly weakened after NCOA2 knockdown. However, NCOA2 knockdown did not influence STAT5 protein level (Figure 8D). ChIP experimental results showed that IL-15 treatment significantly increased the binding of STAT5 protein to the DNA in the promoter region of the *EFNA1* gene, and this binding was weakened after NCOA2 knockdown, indicating that NCOA2 can promote the binding of STAT5 to the *EFNA1* gene (Figure 8E). Functionally, CCK8 and EdU staining experiments showed that IL-15 treatment could significantly increase the proliferation ability of hRMECs and HUVECs, and this increase in proliferation ability was significantly reversed after NCOA2 knockdown (Figure 8F, G). The cell wound-healing assay (Figure 8H, I) and angiogenesis experiment (Figure 8J) also showed similar results, indicating that the promoting effect of IL-15 was weakened after NCOA2 knockdown. In summary, our findings reveal that NCOA2 acts as a transcriptional activator to promote IL-15–induced STAT5 binding to EFNA1 and interacts with EFNA1 in a positive feedback manner, thereby regulating the proliferation, migration, and angiogenic ability of retinal endothelial cells.

DISCUSSION

This study has uncovered the critical role of macrophage-secreted IL-15 in DR, particularly in the regulation of retinal endothelial cell function under HG conditions. The findings indicate that IL-15 is highly expressed in patients with DR and promotes the proliferation, migration, and angiogenesis of vascular endothelial cells, with its effects being enhanced in an HG environment. Further investigation revealed that IL-15 enhances the promotional effect of STAT5 on EFNA1 by activating the STAT5/EFNA1 signaling axis, with the assistance of the transcriptional coactivator NCOA2, thereby affecting the function of retinal endothelial cells. These discoveries provide a new perspective for understanding the pathophysiological mechanisms of DR and offer potential targets for the development of new therapeutic strategies for DR.

This study validated that HG stimulation significantly increased the expression of IL-15 in macrophages. IL-15, a key immunomodulatory factor, not only promotes the activation and proliferation of T cells and NK cells, participating in immune responses, but also plays a vital role in angiogenesis, apoptosis, and inflammatory reactions. Sato and colleagues [29] also found that the level of IL-15 in the vitreous of premature infants with active retinopathy of prematurity is elevated, which may be involved in the process of angiogenesis in ischemic diseases such as diabetes and retinopathy of prematurity. Our study also showed that IL-15 can significantly promote the proliferation, migration, and angiogenesis of retinal endothelial cells under HG conditions in vitro experiments. In the coculture system of macrophages and retinal endothelial cells, the HG environment enhanced the angiogenic capacity of endothelial cells, whereas the absence of IL-15 could significantly offset the angiogenic promotion induced by HG-treated macrophages. This suggests that under HG conditions, macrophage-secreted IL-15 promotes angiogenesis in retinal endothelial cells. However, the specific mechanism by which IL-15 affects angiogenesis in retinal endothelial cells under HG conditions remains unclear.

IL-15 is a pivotal immunomodulatory cytokine that operates by activating the JAK/STAT signaling cascade in diverse cell types. Studies have demonstrated that IL-15 can trigger the JAK/STAT signaling pathway in cultured podocytes through a mechanism dependent on the common γ-chain [30]. Disruption of IL-15 signaling in the colon has been linked to reduced STAT5 phosphorylation in Treg cells, which may contribute to the development of inflammatory bowel disease [31]. It is important to note that excessive activation of the IL-15/STAT5 pathway can elicit cytotoxic responses from ILC1 cells [30]. Additionally, research has indicated that in retinal epithelial cells subjected to HG conditions, there is a significant upregulation of mRNA and secreted protein levels for p-JAK1, p-JAK2, p-STAT3, and p-STAT5 [32]. In ARPE-19 cells, the activation of the STAT signaling pathway by HG has been associated with increased VEGF expression and the regulation of retinal vascular permeability in diabetic mouse models [33]. While the role of IL-15 has been extensively studied across various pathologies, the impact of the IL-15/STAT5 signaling axis on DR remains less elucidated. Through bioinformatics analysis, we found that STAT5A and EFNA1 show the highest significant correlation in the DR group compared to the normal control group. Subsequent experimental findings demonstrated that coculture of macrophages with retinal endothelial cells under HG conditions resulted in a marked increase in the expression of p-STAT2, p-STAT5, and p-STAT6, with p-STAT5 showing the most pronounced upregulation. The expression of these phosphorylated STAT proteins was reversed by knocking out IL-15 in macrophages, which is in line with previous research on the IL-15/STAT5 pathway.

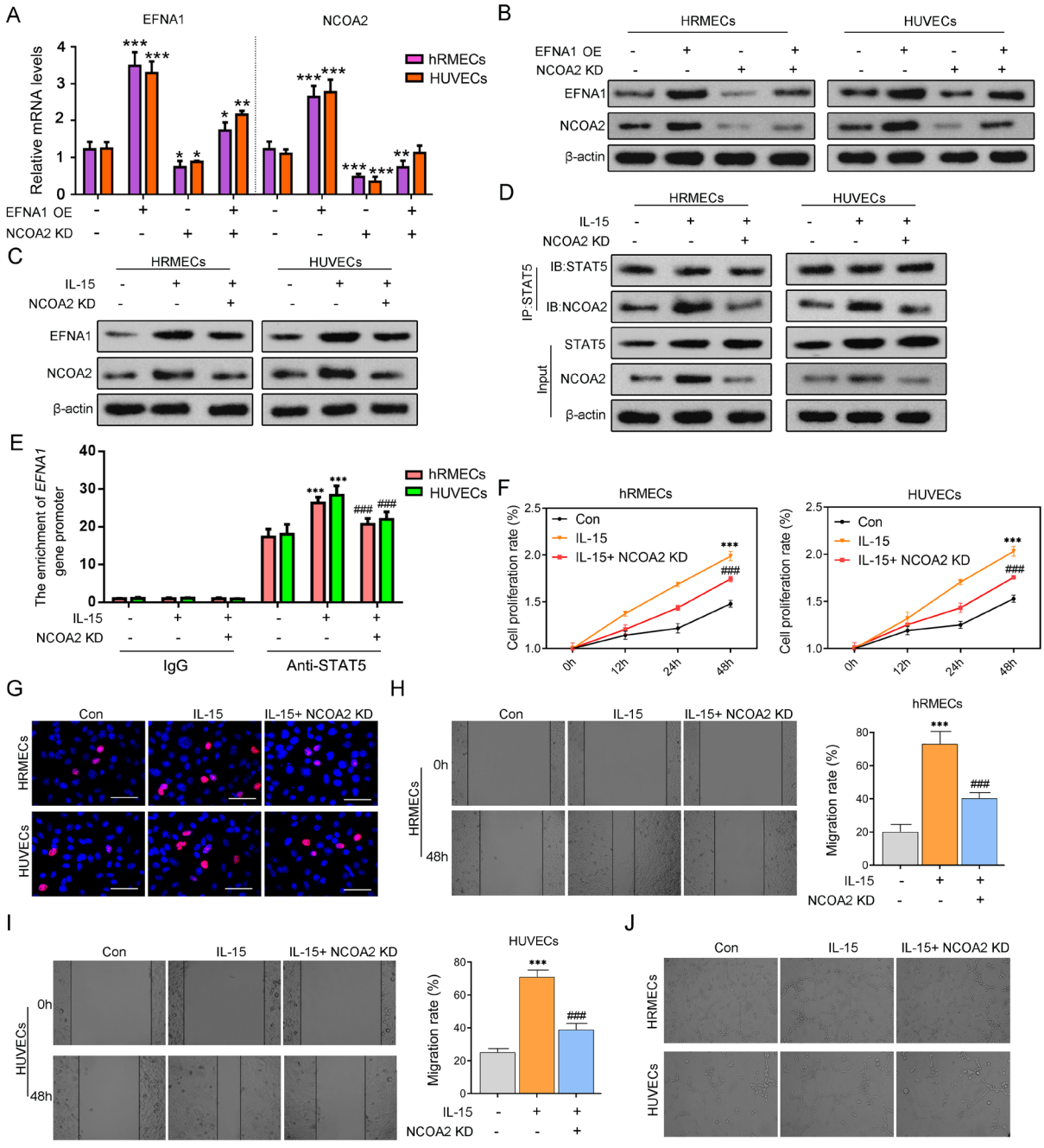

Figure 8. NCOA2 as a transcriptional coactivator induces positive feedback regulation of STAT5/EFNA1. **A**. HRMECs and HUVECs were overexpressed with EFNA1 and transfected with siRNA-NCOA2. Quantitative real-time PCR was used to detect the mRNA expression levels of EFNA1 and NCOA2. **B**. WB experiment was used to detect the protein expression levels of EFNA1 and NCOA2. **C**. Vascular endothelial cells were treated with IL-15 for 48 h, and NCOA2 expression was knocked down. WB experiment was used to detect the protein expression level of EFNA1. **D**. Co-immunoprecipitation experiment was used to validate the interaction between STAT5 and NCOA2. **E**. ChIP experiment was used to validate the binding relationship between STAT5 protein and the EFNA1 gene. **F**. CCK8 was used to detect the cell proliferation rate of vascular endothelial cells cultured for 0, 12, 24, and 48 h. **G**. EdU staining was used to assess cell proliferation ability. **H, I**. The cell wound-healing assay was used to detect cell migration ability. **J**. The angiogenesis assay was used to detect tubule formation ability. *$p < 0.05$, **$p < 0.01$, ***$p < 0.001$ versus Con. #$p < 0.05$, ##$p < 0.01$, ###$p < 0.001$ versus IL-15. n = 3. Statistical significance was determined by using one-way analysis of variance for more than two groups. Subsequently, Dunnett's post hoc tests were conducted. $p < 0.05$ was considered significant.

Ephrin (EFN), the ligand for the Eph receptor, is divided into two subgroups based on their attachment to the membrane: the FNA family (EFNA1–5) is attached via glycosylphosphatidylinositol linkage, while the EFNB family (EFNB1–3) is anchored through a transmembrane protein domain [34]. Studies have shown that EFNA1 can activate the EphA2 receptor, which in turn recruits and binds to Vav2. Activated Vav proteins promote the activation of Rac1, thereby enhancing the migration ability of endothelial cells and the process of vascular assembly [34], as well as participating in angiogenesis [35]. Additionally, activated EphA2 receptors bind and activate PI3K, upregulate PIP3 levels, further enhance the activation of the Vav family, and promote angiogenesis. Deficiencies in PI3K and Rac1 would impair the migration of endothelial cells induced by EFNA1 [36]. In vitro experiments have shown that the deficiency of EFNA1 after specific siRNA treatment is associated with reduced migration of vascular endothelial cells. EFNA1 has a broad impact on the occurrence and development of various diseases through the regulation of angiogenesis in vivo. Recent studies have found that EFNA1 can stimulate endothelial cell migration and induce corneal angiogenesis [37], and it may be a more sensitive biomarker than plasma VEGF165 for detecting DR [38]. Our study found that after treating endothelial cells with IL-15, the expression of both STAT5 and EFNA1 increased, and the cell proliferation, migration, and angiogenesis abilities were enhanced. Knocking down STAT5 expression significantly reversed the IL-15–induced increase in STAT5 and EFNA1 and the function of retinal endothelial cells. Additionally, EFNA1 is highly expressed in retinal endothelial cells induced by HG, and the expression of p-AKT and p-Vav is also elevated. After knocking down EFNA1 expression, the expression of EFNA1, p-AKT, and p-Vav was reversed, indicating that EFNA1 may be one of the important targets for treating angiogenesis in DR, which is consistent with previous research findings. As a transcription factor, we speculate that STAT5 may affect the angiogenic ability of DR by regulating the transcriptional expression of EFNA1. To further understand the mechanism by which STAT5 regulates EFNA1, we used ChIP experiments to validate the binding of STAT5 to the EFNA1 gene. The results indicate that STAT5 regulates the angiogenic ability of retinal endothelial cells by modulating EFNA1 transcription.

In the bioinformatics analysis of the DR database, we found a significant correlation between NCOA2 and EFNA1. NCOA2 is a member of the NCOA coactivator family [39], which functions not by directly binding to target DNA but by serving as a coactivator for steroid nuclear receptors and other transcription factors, thereby regulating gene transcription [38]. Previous studies have shown that NcoA2 can form complexes with KAT2B (lysine acetyltransferase 2B) and subunits of NF-κB (p50 and p65), thereby activating the transcription of related genes and promoting inflammatory responses [38]. Moreover, NCOA2 is recruited by CREB to the PGC1A (PGC-1α) gene locus, enhancing PGC-1α gene expression and subsequently influencing mitochondrial metabolic functions [38]. Although NCOA2 has been demonstrated to regulate various physiologic processes, its role in ophthalmic diseases remains partially undefined. Studies suggest that under hypoxia-mimicking conditions, NCOA2 can influence angiogenesis by modulating the interaction between the aryl hydrocarbon receptor and hypoxia-inducible factor 1α [40]. We hypothesize that NcoA2 can be recruited by STAT5 to form a transcriptional complex, thereby stimulating EFNA1 expression. Subsequent in vitro experiments found that NCOA2, as a transcriptional coactivator, promotes the transcriptional activity of STAT5 on EFNA1, thereby enhancing the proliferation, migration, and angiogenesis abilities of retinal endothelial cells. Moreover, NCOA2 and EFNA1 positively modulated each other, synergistically mediating IL-15's regulation of retinal endothelial cell angiogenesis.

This study also has certain limitations. First, the clinical sample size used in our study is relatively small, which may affect the statistical results. Future research will aim to increase the sample size to enhance the reliability and clinical relevance of the findings. Second, our study lacks in vivo experimental data to validate the findings from in vitro experiments. In vivo experiments can more realistically simulate the pathological environment of DR, and future research will consider further validating the role of IL-15 on the STAT5/NCOA2/EFNA1 signaling axis in DR animal models.

In conclusion, our research indicates that under HG conditions, macrophage-secreted IL-15 activates STAT5, which in turn induces positive feedback regulation of EFNA1/NCOA2, thereby promoting retinal angiogenesis. These findings provide a new perspective for understanding the molecular mechanisms of DR and may offer important targets for the development of therapeutic strategies for DR.

APPENDIX 1. STR ANALYSIS.

To access the data, click or select the words "Appendix 1." STR analysis of THP-1, RMEC and HUVEC.

APPENDIX 2. SUPPLEMENTARY FIGURE 1. THE KNOCKOUT AND KNOCKDOWN OF GENES.

To access the data, click or select the words "Appendix 2." To induce IL-15 knockout, we employed the CRISPR/Cas9 technology. Initially, we designed and synthesized a single guide RNA (sgRNA) sequence targeting a conserved region within the coding region of the *IL-15* gene. **A–C**. The knockout of the *IL-15* gene in THP-1 was validated by PCR and western blot tests. This study designed three small interfering RNAs (siRNAs) for each STAT5, EFNA1, and NCOA2 mRNA. **D–F**. PCR was conducted to evaluate the efficiency of these siRNAs on the knockdown of STAT5, EFNA1, and NCOA2. *$p < 0.05$, **$p < 0.01$, ***$p < 0.001$ versus Con. #$p < 0.05$, ##$p < 0.01$, ###$p < 0.001$ versus IL-15. n = 3. Statistical significance was determined by using an unpaired Student *t* test for two groups or one-way analysis of variance for more than two groups. Subsequently, Dunnett's post hoc tests were conducted. $p < 0.05$ was considered significant.

ACKNOWLEDGMENTS

Funding: This work was supported by the Hunan Provincial Natural Science Foundation Project (No.2022JJ30321), Project of Hunan Provincial Department of Science and Technology (202107022320), Hunan Children's Eye Disease Screening and Prevention Clinical Medical Research Center (2023SK4044) and Changsha Major Science and Technology Project (kh2401012). Conflict of Interest: There are no conflicts of interest. Authors' contribution: Study concept and design: Lixin Zhang and Yan Guo; data acquisition: Lixin Zhang and Yan Guo; data analysis and interpretation: Lixin Zhang and Yan Guo; drafting of the manuscript: Lixin Zhang and Yan Guo; statistical analysis: Lixin Zhang and Yan Guo; study supervision: Lixin Zhang and Yan Guo. Data availability: The data in this study can be obtained from the corresponding author. Ethical approval: Our research obtained approval from the Ethics Committee of Hunan Children's Hospital (approval number: 2022–303), and research was conducted in accordance with the Declaration of Helsinki. Informed consent: All patients obtained informed consent for pathological examination and signed informed consent.

REFERENCES

1. Sheetz MJ, King GL. Molecular understanding of hyperglycemia's adverse effects for diabetic complications. JAMA. 2002; 288:2579-88. [PMID: 12444865].

2. Spranger J, Pfeiffer AF. New concepts in pathogenesis and treatment of diabetic retinopathy. Exp Clin Endocrinol Diabetes 2001; 109:Suppl 2S438-50. [PMID: 11460590].

3. Teo ZL, Tham YC, Yu M, Chee ML, Rim TH, Cheung N, Bikbov MM, Wang YX, Tang Y, Lu Y, Wong IY, Ting DSW, Tan GSW, Jonas JB, Sabanayagam C, Wong TY, Cheng CY. Global prevalence of diabetic retinopathy and projection of burden through 2045: systematic review and meta-analysis. Ophthalmology. 2021; 128:1580-91. [PMID: 33940045].

4. Solomon SD, Chew E, Duh EJ, Sobrin L, Sun JK, VanderBeek BL, Wykoff CC, Gardner TW. Erratum. Diabetic retinopathy: a position statement by the American Diabetes Association. Diabetes Care 2017;40:412-418. Diabetes Care. 2017; 40:809-[PMID: 28432087].

5. Lin KY, Hsih WH, Lin YB, Wen CY, Chang TJ. Update in the epidemiology, risk factors, screening, and treatment of diabetic retinopathy. J Diabetes Investig. 2021; 12:1322-5. [PMID: 33316144].

6. Riabov V, Gudima A, Wang N, Mickley A, Orekhov A, Kzhyshkowska J. Role of tumor associated macrophages in tumor angiogenesis and lymphangiogenesis. Front Physiol. 2014; 5:75-[PMID: 24634660].

7. Abdelfattah NS, Amgad M, Zayed AA. Host immune cellular reactions in corneal neovascularization. Int J Ophthalmol. 2016; 9:625-33. [PMID: 27162740].

8. Yim SY, Lee SH, Baek SW. Sohn B, Jeong YS, Kang SH, Park K, Park H, Lee SS, Kaseb AO, Park YN, Leem SH, Curran MA, Kim JH, Lee JS et al.. Genomic biomarkers to predict response to atezolizumab plus bevacizumab immunotherapy in hepatocellular carcinoma: insights from the IMbrave150 Trial. Clin Mol Hepatol. 2024 ;30:807–823. PMID: 39038962

9. Shen T, Lin R, Hu C, Yu D, Ren C, Li T, Zhu M, Wan Z, Su T, Wu Y, Cai W, Yu J. Succinate-induced macrophage polarization and RBP4 secretion promote vascular sprouting in ocular neovascularization. J Neuroinflammation. 2023; 20:308-[PMID: 38129891].

10. Guo Y, Zhang C, Xie B, Xu W, Rao Z, Zhou P, Ma X, Chen J, Cai R, Tao G, He Y. Multifunctional microneedle patch based on metal-phenolic network with photothermal antimicrobial, ROS scavenging, immunomodulatory, and angiogenesis for programmed treatment of diabetic wound healing. ACS Appl Mater Interfaces. 2024; 16:33205-22. [PMID: 38915205].

11. Lee SJ, Noh SE, Jo DH, Cho CS, Park KS, Kim JH. IL-10-induced modulation of macrophage polarization suppresses outer-blood-retinal barrier disruption in the streptozotocin-induced early diabetic retinopathy mouse model. FASEB J. 2024; 38:e23638[PMID: 38713098].

12. Liu G, Wu H, Lu P, Zhang X. Interleukin (IL)-17A promotes angiogenesis in an experimental corneal neovascularization model. Curr Eye Res. 2017; 42:368-79. [PMID: 27419340].

13. De Luisi A, Binetti L, Ria R, Ruggieri S, Berardi S, Catacchio I, Racanelli V, Pavone V, Rossini B, Vacca A, Ribatti D. Erythropoietin is involved in the angiogenic potential of bone marrow macrophages in multiple myeloma. Angiogenesis. 2013; 16:963-73. [PMID: 23881169].

14. Gordon SM, Nishiguchi MA, Chase JM, Mani S, Mainigi MA, Behrens EM. IFNs drive development of novel

IL-15-responsive macrophages. J Immunol 2020; 205:1113-24. [PMID: 32690654].

15. Nandi M, Moyo MM, Orkhis S, Mobulakani JMF, Limoges MA, Rexhepi F, Mayhue M, Cayarga AA, Marrero GC, Ilangumaran S, Menendez A, Ramanathan S. IL-15Rα-independent IL-15 signaling in non-NK cell-derived IFNγ driven control of *Listeria monocytogenes*. Front Immunol. 2021; 12:793918[PMID: 34956227].

16. Cui G, Hara T, Simmons S, Wagatsuma K, Abe A, Miyachi H, Kitano S, Ishii M, Tani-ichi S, Ikuta K. Characterization of the IL-15 niche in primary and secondary lymphoid organs in vivo. Proc Natl Acad Sci U S A. 2014; 111:1915-20. [PMID: 24449915].

17. Biber JL, Jabbour S, Parihar R, Dierksheide J, Hu Y, Baumann H, Bouchard P, Caligiuri MA, Carson W. Administration of two macrophage-derived interferon-gamma-inducing factors (IL-12 and IL-15) induces a lethal systemic inflammatory response in mice that is dependent on natural killer cells but does not require interferon-gamma. Cell Immunol. 2002; 216:31-42. [PMID: 12381348].

18. Angiolillo AL, Kanegane H, Sgadari C, Reaman GH, Tosato G. Interleukin-15 promotes angiogenesis in vivo. Biochem Biophys Res Commun. 1997; 233:231-7. [PMID: 9144429].

19. Zhang Q, Zhang J, Wang P, Zhu G, Jin G, Liu F. Glioma-associated mesenchymal stem cells-mediated PD-L1 expression is attenuated by Ad5-Ki67/IL-15 in GBM treatment. Stem Cell Res Ther. 2022; 13:284-[PMID: 35765095].

20. Tremblay CS, Saw J, Boyle JA, Haigh K, Litalien V, McCalmont H, Evans K, Lock RB, Jane SM, Haigh JJ, Curtis DJ. STAT5 activation promotes progression and chemotherapy resistance in early T-cell precursor acute lymphoblastic leukemia. Blood. 2023; 142:274-89. [PMID: 36989489].

21. Pandiyan P, Yang XP, Saravanamuthu SS, Zheng L, Ishihara S, O'Shea JJ, Lenardo MJ. The role of IL-15 in activating STAT5 and fine-tuning IL-17A production in CD4 T lymphocytes. J Immunol 2012; 189:4237-46. [PMID: 22993203].

22. Carbajo-Pescador S, Ordoñez R, Benet M, Jover R, García-Palomo A, Mauriz JL, González-Gallego J. Inhibition of VEGF expression through blockade of Hif1α and STAT3 signalling mediates the anti-angiogenic effect of melatonin in HepG2 liver cancer cells. Br J Cancer. 2013; 109:83-91. [PMID: 23756865].

23. Lombardo G, Dentelli P, Togliatto G, Rosso A, Gili M, Gallo S, Deregibus MC, Camussi G, Brizzi MF. Activated Stat5 trafficking via endothelial cell-derived extracellular vesicles controls IL-3 pro-angiogenic paracrine action. Sci Rep. 2016; 6:25689-[PMID: 27157262].

24. Su L, Xie S, Li T, Jia Y, Wang Y. Pretreatment with platelet-rich plasma protects against ischemia-reperfusion induced flap injury by deactivating the JAK/STAT pathway in mice. Mol Med. 2024; 30:18-[PMID: 38302877].

25. Cavazzoni A, Digiacomo G, Volta F, Alfieri R, Giovannetti E, Gnetti L, Bellini L, Galetti M, Fumarola C, Xu G, Bonelli M, La Monica S, Verzè M, Leonetti A, Eltayeb K, D'Agnelli S, Moron Dalla Tor L, Minari R, Petronini PG, Tiseo M. PD-L1 overexpression induces STAT signaling and promotes the secretion of pro-angiogenic cytokines in non-small cell lung cancer (NSCLC). Lung Cancer. 2024; 187:107438[PMID: 38100954].

26. Dudley AC, Thomas D, Best J, Jenkins A. A VEGF/JAK2/STAT5 axis may partially mediate endothelial cell tolerance to hypoxia. Biochem J. 2005; 390:427-36. [PMID: 15918795].

27. Tian M, Qi Y, Zhang X, Wu Z, Chen J, Chen F, Guan W, Zhang S. Regulation of the JAK2-STAT5 pathway by signaling molecules in the mammary gland. Front Cell Dev Biol. 2020; 8:604896[PMID: 33282878].

28. Livak KJ, Schmittgen TD. Analysis of relative gene expression data using real-time quantitative PCR and the 2(-Delta Delta C(T)) method. Methods. 2001; 25:402-8. [PMID: 11846609].

29. Sato T, Kusaka S, Shimojo H, Fujikado T. Simultaneous analyses of vitreous levels of 27 cytokines in eyes with retinopathy of prematurity. Ophthalmology. 2009; 116:2165-9. [PMID: 19700197].

30. Zhang Y, Zhao L, Wu A, Lin P, Fan J, Chen J, Wang X, Zeng X. Abnormal M1 polarization of placental macrophage induced by IL-15/STAT5 activation in VVC may lead to adverse pregnancy outcomes. Microbes Infect. 2024; 26:105232[PMID: 37802467].

31. Nixon BG, Chou C, Krishna C, Dadi S, Michel AO, Cornish AE, Kansler ER, Do MH, Wang X, Capistrano KJ, Rudensky AY, Leslie CS, Li MO. Cytotoxic granzyme C-expressing ILC1s contribute to antitumor immunity and neonatal autoimmunity. Sci Immunol. 2022; 7:eabi8642[PMID: 35394814].

32. Cho CH, Roh KH, Lim NY, Park SJ, Park S, Kim HW. Role of the JAK/STAT pathway in a streptozotocin-induced diabetic retinopathy mouse model. Graefes Arch Clin Exp Ophthalmol. 2022; 260:3553-63. [PMID: 35599279].

33. Kim HW, Kim JL, Lee HK, Hur DY, Yun IH, Kim SD. Enalapril alters expression of key growth factors in experimental diabetic retinopathy. Curr Eye Res. 2009; 34:976-87. [PMID: 19958114].

34. Hao Y, Li G. Role of EFNA1 in tumorigenesis and prospects for cancer therapy. Biomed Pharmacother. 2020; 130:110567[PMID: 32745910].

35. Hunter SG, Zhuang G, Brantley-Sieders D, Swat W, Cowan CW, Chen J. Essential role of Vav family guanine nucleotide exchange factors in EphA receptor-mediated angiogenesis. Mol Cell Biol. 2006; 26:4830-42. [PMID: 16782872].

36. Shuai Q, Xu X, Liang Y, Halbiyat Z, Lu X, Hu Z, Peng Z, An J, Feng Z, Huang T, Zhao H, Liu Z, Xu J, Xie J. Engineered in vivo and in vitro tumor model recapitulates vasculogenic mimicry signatures in melanoma. Bioeng Transl Med. 2024; 9:e10648[PMID: 39036079].

37. Khan N, Kumar V, Li P, Schlapbach LJ, Boyd AW, Coulthard MG, Woodruff TM. RAPIDS Study Group. Inhibiting Eph/ephrin signaling reduces vascular leak and endothelial cell dysfunction in mice with sepsis. Sci Transl Med. 2024; 16:eadg5768[PMID: 38657024].

38. Zhong X, Wu H, Ouyang C, Zhang W, Shi Y, Wang YC, Ann DK, Gwack Y, Shang W, Sun Z. Ncoa2 promotes CD8+ T cell-mediated antitumor immunity by stimulating T-cell activation via upregulation of PGC-1α critical for mitochondrial function. Cancer Immunol Res. 2023; 11:1414-31. [PMID: 37540802].

39. Tay WJ, Jeyasekharan A, Goh JY, Chang KTE, Kesavan A, Lee VK. Aggressive prostate myxoid mesenchymal neoplasm with novel CRTC1:NCOA2 fusion. Histopathology. 2024; 84:909-12. [PMID: 38173295].

40. Tsai CH, Li CH, Liao PL, Cheng YW, Lin CH, Huang SH, Kang JJ. NcoA2-dependent inhibition of HIF-1α activation is regulated via AhR. Toxicol Sci 2015; 148:517-30. [PMID: 26350169].

Articles are provided courtesy of Emory University and The Abraham J. & Phyllis Katz Foundation. The print version of this article was created on 31 December 2025. This reflects all typographical corrections and errata to the article through that date. Details of any changes may be found in the online version of the article.